

DIGITAL MOTION ANALYSIS AS A TOOL FOR ANALYSING THE SHAPE AND PERFORMANCE OF THE CIRCULATORY SYSTEM IN TRANSPARENT ANIMALS

THORSTEN SCHWERTE* AND BERND PELSTER

Department of Zoology, University of Innsbruck, A-6020 Innsbruck, Austria

*Present address: Institut für Zoologie und Limnologie, Leopold-Franzens-Universität, Techniker Straße 25, A-6020 Innsbruck, Austria
(e-mail: thorsten.schwerte@uibk.ac.at)

Accepted 15 March; published on WWW 10 May 2000

Summary

The analysis of perfusion parameters using the frame-to-frame technique and the observation of small blood vessels in transparent animals using video microscopy can be tedious and very difficult because of the poor contrast of the images. Injection of a fluorescent probe (fluorescein isothiocyanate, FITC) bound to a high-molecular-mass dextran improved the visibility of blood vessels, but the gray-scale histogram showed blurring at the edges of the vessels. Furthermore, injection of the fluorescent probe into the ventricle of small zebrafish (*Danio rerio*) embryos (body mass approximately 1 mg) often resulted in reduced cardiac activity. Digital motion analysis, however, proved to be a very effective tool for analysing the shape and performance of the circulatory system in transparent animals and tissues. By subtracting the two fields of a video frame (the odd and the even frame), any movement that occurred within the 20 ms necessary for the acquisition of one field could be visualised. The length of the shifting vector generated by this subtraction, represented a direct measure of the velocity of a moving particle, i.e. an erythrocyte in the vascular system. By accumulating

shifting vectors generated from several consecutive video frames, a complete trace of the routes over which erythrocytes moved could be obtained. Thus, a cast of the vascular system, except for those tiny vessels that are not entered by erythrocytes, could be obtained. Because the gray-scale value of any given pixel or any given group of pixels increased with the number of erythrocytes passing it, digital motion analysis could also be used to visualise the distribution of blood cells in transparent tissues. This method was used to describe the development of the peripheral vascular system in zebrafish larvae up to 8 days post-fertilisation. At this stage, food intake resulted in a clear redistribution of blood between muscle tissue and the gut, and α -adrenergic control of peripheral blood flow was established.

Key words: video image analysis, digital motion analysis, erythrocyte count, erythrocyte velocity, blood flow, microcirculation, cardiovascular system, development, zebrafish, *Danio rerio*, European eel, *Anguilla anguilla*, adrenaline.

Introduction

The use of photographic cine film images to analyse physiological events dates back several decades, but with respect to the documentation of circulatory phenomena or cardiac activity it became an important tool in the 1960s and 1970s. One of the first applications was probably the measurement of skin perfusion in humans using a so-called videocapillary microscope with frame-to-frame analysis (Fagrell et al., 1977; Hudetz, 1997), and both this method and the laser Doppler system were very soon used in comparative animal physiology (Koyama et al., 1975; Farrell et al., 1980; Hughes et al., 1981). Within recent years, video imaging has become the main tool for the analysis of cardiac performance in transparent amphibian and fish embryos and larvae (Faber et al., 1974; Burggren and Fritsche, 1995; Colmorgen and Paul, 1995; Hou and Burggren, 1995; Orlando and Pinder, 1995; Fritsche and Burggren, 1996; Keller et al., 1996).

The experimental procedure is quite simple: one needs a

dissecting microscope or a microscope with a video adapter and a video recorder. Video recordings are then made of a beating heart or of moving blood cells, and these recordings are analysed using the replay mode and slow-motion facilities. This observer-dependent and time-consuming method provides information about red cell velocity and blood flow (Pelster and Bemis, 1992) and about heart rate, stroke volume and cardiac output (see Burggren and Fritsche, 1995). A more advanced method includes the digitisation of images using a frame-grabber card and subsequent processing of the images using computer programs such as Adobe Photoshop (MacFarlane et al., 1983; Vesely et al., 1990; Sundin, 1995; Nilsson et al., 1995; Sundin and Nilsson, 1997; Hudetz, 1997). Although digitisation makes the analysis procedure easier, it still remains an observer-dependent method in which the result may vary with the illumination and contrast of the video image. The determination of vessel diameter is particularly difficult

because the vessel walls often disappear in still images of transparent tissues (Hanger et al., 1995), and in fish gills, for example, the visibility of the cell membrane of pillar cells depends on the presence of moving erythrocytes (Stensløkken et al., 1999).

The fact that the visibility of blood vessel walls in most transparent tissues is dependent on the presence of moving erythrocytes led us to the idea of visualising the movement of floating erythrocytes by generating a difference image from the odd and even fields of a video frame. This manipulation permits not only an elegant and easy determination of erythrocyte velocities but, by summing several difference images, also a visualisation of the vascular system and of the distribution of erythrocytes within the vascular bed.

Materials and methods

The experiments were performed using the almost transparent swimbladder tissue of the European eel and various larval stages of the zebrafish. European eels (*Anguilla anguilla*) were obtained from a local supplier and kept in a freshwater aquarium at 12 °C. Experiments with eels were performed at 20±1 °C. Zebrafish (*Danio rerio*) larvae were obtained from our own breeding colony. Because of their greater transparency, poorly pigmented mutants of the zebrafish (Albino, Brass, Transparent) were used. Parent animals used to start the breeding colonies were either obtained from a local supplier or generously provided by Dr Frohnhöfer from the Max-Planck Institute for Developmental Biology in Tübingen and Ms Loos from the University of Konstanz. Breeding colonies and larvae were kept in small aquaria at 28 °C. From day 6 post-fertilisation, the animals were fed with a fine nutrient powder. Experiments with zebrafish larvae were performed at 28 °C.

Animal preparations and perfusion experiments in the eel

Anaesthetised eels were quickly immobilised by penetrating the skull with a fine needle and spinal pithing. The animals were placed into an eel-holder (Schwerte et al., 1997), and the gills were irrigated with well-aerated water (20–22 °C) at a constant flow of approximately 1.5–2 l min⁻¹. The body wall was opened ventrally. The swimbladder was carefully exposed and freed of connective tissue. Blood vessels from other tissues entering the vein leaving the retia were ligated.

To perfuse the swimbladder with blood, the swimbladder artery was occlusively catheterised and the dorsal artery was cannulated non-occlusively (PE 50). Blood was drawn from the dorsal artery and infused into the swimbladder artery at a constant flow rate. Thus, after swimbladder perfusion, the blood was returned to the central circulation and reoxygenated in the gills. Catheter tubing was heparinized with 100 i.u. ml⁻¹ saline (see Pelster, 1994). Video recordings were made using a Leica MZ8 dissection microscope with an attached black-and-white CCD camera. The tissue was illuminated from the side to enhance image contrast due to light reflection from the erythrocytes.

Mounting of zebrafish larvae

For the experiments, embryos and larvae of the zebrafish 2–21 days post-fertilisation were used. The animals were anaesthetised by adding 50 mg l⁻¹ phosphate-buffered tricaine (MS222; pH 7.0) to the water. After 1 min of anaesthesia, the animals were removed and carefully mounted in the experimental chamber with a thin layer (100–200 µm) of 1 % low-melting-point agarose (Sea Plaque; gelling point 26–30 °C), containing 50 mg l⁻¹ phosphate-buffered tricaine. The gel was covered with air-equilibrated water containing 50 mg l⁻¹ phosphate-buffered tricaine. This chamber was transferred into the temperature-controlled microscope desk of an inverted microscope (Zeiss Axiovert 25CF). The inverted microscope allows a plane view of the ventral or lateral side of the larvae. The left side of the animal provided the best view of the central cardiac system.

Application of phenylephrine

To test for the presence of α-adrenergic receptors, a micropipette was used to eject 300 µl of a 10⁻⁶ mol l⁻¹ solution of the α-adrenergic agonist phenylephrine within 10 s very close to an intersegmental vessel in the tail region of zebrafish larvae. The mucus on the skin was removed carefully using a broken micropipette 5 min before acquiring control data.

The imaging system

To reduce vibratory movements, the inverted microscope was placed on a solid heavy-weight steel plate. The illumination could be set to infrared light with a wavelength of 780 or 913 nm to prevent light-induced stress reactions of the animals. The microscope was equipped with a 2/3 inch monochrome machine vision CCD camera (M300, JAI, Copenhagen/Denmark; without infrared cut-off filter), which in turn was connected to the luminance input (the chrominance input was left unconnected) of an SVHS video recorder (Sony S-9500). The video recorder was remotely controlled via the RS232 serial communication port. The setting of the video recorder and the recorded images were digitised using a monochrome frame-grabber card (PX-610, Imagenation, Beaverton, USA) with a personal computer (PIII 450 MHz). All measurements and image enhancement procedures were performed using custom-made Analytical Language for Images (ALI) programs running on the Optimas 6.5 programming platform (Media Cybernetics, Silver Springs, USA). The analytical procedures were optimised for automatically exporting data and enhanced images to files. Some of the data were acquired in real time, while the video recorder stored the video data for archiving purposes. This was strictly necessary for measurements in tiny vessels because the signal from the video recorder was too noisy for appropriate resolution.

Measurement of erythrocyte velocity by digital motion analysis

A frame from an interlaced standard CCD video camera consists of two fields. The first field contains all odd lines and

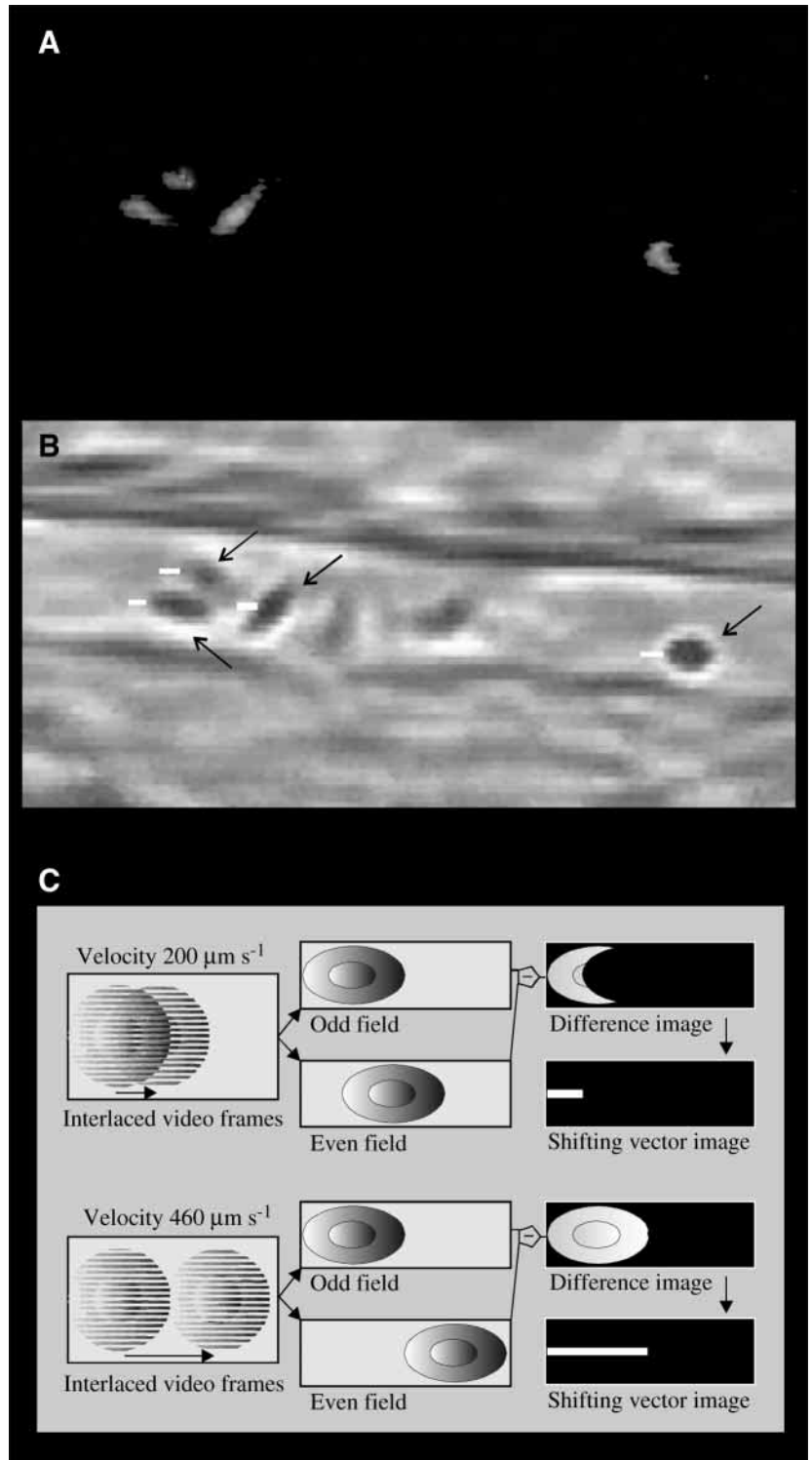


Fig. 1. The basic principle of digital motion analysis. (A) A difference image obtained by subtracting the two fields of one video frame (the odd and the even frame), showing four moving erythrocytes. (B) The original video frame showing erythrocytes flowing within a $12 \mu\text{m}$ diameter capillary. This image was used to generate the difference picture. The arrows point to the moving cells and the white bars represent the shifting vectors. (C) A schematic drawing showing a moving erythrocyte and the shifting vector, which is a measure of the distance travelled by the cell within the 20 ms necessary to acquire one field of a video frame.

the second field all even lines. The acquisition of each field takes 20 ms. The pixels within each field can be separated into static pixels, located in non-moving areas of the image where no change in gray-scale occurs compared with the subsequent field, and dynamic pixels, located in areas where movement occurs and changes in gray-scale compared with the following field take place. In consecutive fields, the gray-scale value of any pixel in a static area remains constant, while the gray-scale

value of a pixel in an area where movement occurs changes. Thus, subtraction of the contents of two consecutive fields (with elimination of negative values) results in a clear separation of the static pixel and half the dynamic pixels. In a static area, the subtraction of two consecutive fields results in a gray-scale value of zero (black), while any dynamic pixel will differ from black with a gray-scale value ranging from 1 (dark gray) to 255 (white).

The sum of all dynamic pixels on a horizontal line derived from the movement of a single object (a red cell, for example) is called the shifting vector, and the length of this shifting vector represents the distance travelled by the object. Fig. 1 illustrates the generation of shifting vectors for erythrocytes floating in the bloodstream. To gain most advantage from the shifting vectors produced by interlaced video images, the movement of the erythrocytes projected onto the camera chip should occur along an axis parallel to the lines of the CCD chip. Because the length of the shifting vector represents a measure of the velocity of the object, and not the gray-scale value, the contrast of images including all shifting vectors was enhanced by application of a 3×3 median filter and subsequent binarization, which turns all pixels with a gray value higher than 1 to white. The maximum detectable velocity V_{\max} (in ms) is dependent on the visual diameter of the object projection D_{object} :

$$V_{\max} = D_{\text{object}}/20.$$

Because the maximum detectable velocity is greatest in a median section of a round erythrocyte (see also Fig. 1C), only the shifting vectors from the middle area of a blood cell were used for further analysis. This determination was repeated for all fields for three complete cardiac cycles to obtain a mean value for the velocity of the erythrocyte. Once the region of interest had been defined, complete data extraction from the images was performed automatically.

Visualisation of blood vessels by digital motion analysis

The shifting vectors derived from moving erythrocytes can also be used for contrast enhancement in the vascular system. By summing the visualised non-binarized shifting vectors of a sufficiently large number of frames, a complete outline of all areas in which erythrocyte movement occurred was obtained. This is essentially a cast of the vascular system, except for those tiny capillaries that do not permit the passage of erythrocytes (Fig. 2). The number of repetitions was carefully set to prevent pixel values from exceeding gray value 255 (white).

The difference in gray-scale value between the background and an erythrocyte of a zebrafish larva was between 8 and 12. Therefore, 20–30 repetitions were sufficient to obtain a good image. To improve the image further, a 3×3 median filter was applied, and gray values lower than the number of iterations were discarded to minimise noise.

Measurement of vessel diameter by digital motion analysis

The cast of the vascular bed, obtained by summing the visualised non-binarized shifting vectors of a sufficiently large number of frames, was also used to determine the diameters of blood vessels at any region of interest. In these regions of interest, the boundaries of the blood vessel were detected by a freely defined gray-scale threshold. An algorithm was developed to find a vector that described the properties of a rectangle with the same binary moments as the extracted area found by the defined threshold. The lengths of the major axis and the minor axis were extracted for direct measurement of the diameter and the length of the vessel in the region of interest.

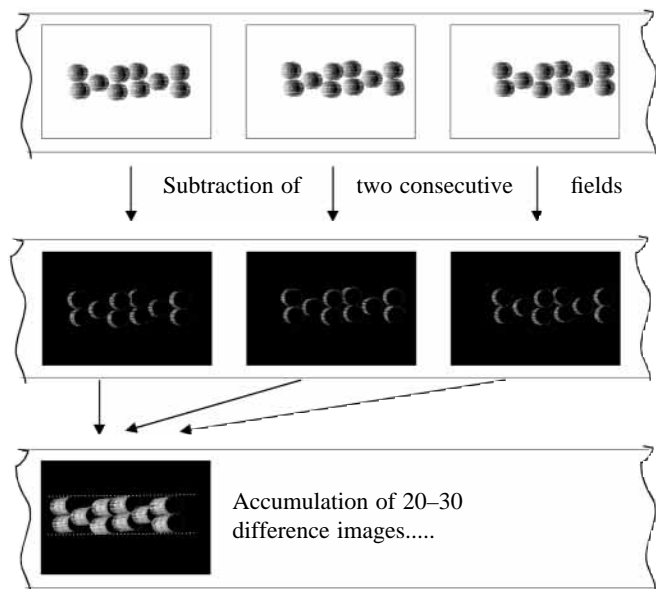


Fig. 2. Visualisation of a blood vessel by accumulation of shifting vectors from consecutive fields. The generation of difference pictures of the two fields of one frame results in the generation of shifting vectors. By superimposing a sufficiently large number of difference images from subsequent frames, a trace of all routes over which erythrocytes have travelled is obtained.

To compensate for minor movements of the animal, a reference point was determined in the vicinity of the measurement site (see below). This reference point was automatically relocated prior to every determination of the vessel diameter. The images used for measurement of vessel diameter were recorded using a 40× phase-contrast objective.

Visualisation of blood distribution

To visualise blood distribution, the shifting vectors were binarized. The process of binarization (the threshold was set from 5 to 12) reduces the image information on the visualisation of so-called events, where an event is the movement of an erythrocyte. By summing these binarized images, the gray-scale value of any given pixel or of a defined number of pixels in the image rises from zero to 255 depending on the number of erythrocytes passing it. The resulting gray-scale value therefore codes the number of erythrocytes that have passed the region of interest. Although the depth of the gray-scale display on the screen is limited to 8 bits, the actual range for the calculations was extended to 24 bits. Thus, differences in blood distribution in whole animals could be visualised in overview images using a 4× phase-contrast objective. The procedure ran automatically, while measurements of erythrocyte distribution could be made

Table 1. *The dimensions of the visible fields and the size of the pixels*

Magnification	Visible field (μm)	Pixel size (μm)
4×	1997×1606	2.603×2.793
40×	257.8×206.4	0.3361×0.3589

automatically in predefined regions of interest. The dimensions of the visible fields and the size of the pixels are listed in Table 1.

Measurement of erythrocyte velocity based on the frame-to-frame technique

In blood vessels smaller than 100 μm in diameter, the velocity of erythrocytes was determined by multiplying the number of frames recorded while an erythrocyte travelled a given distance by 40 ms, the time needed to acquire a whole frame (frame-to-frame technique). The custom-made program automatically displayed the image sequence from the video tape, while the user tracked individual erythrocytes using the mouse. The velocity was calculated and exported automatically. The imaging system was calibrated using an object micrometer. Each measurement was repeated five times, and the readings obtained were averaged to flatten the pulses of the cardiac rhythm.

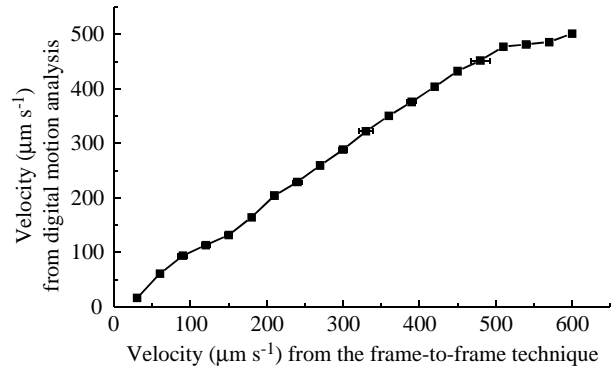


Fig. 3. The velocity of erythrocytes determined on the basis of the shifting vector (digital motion analysis) compared with the velocity determined using the conventional frame-to-frame technique. Note that the velocity determined on the basis of the shifting vector levels off at velocities above 450 $\mu\text{m s}^{-1}$. Values are means \pm S.E.M., $N=17$.

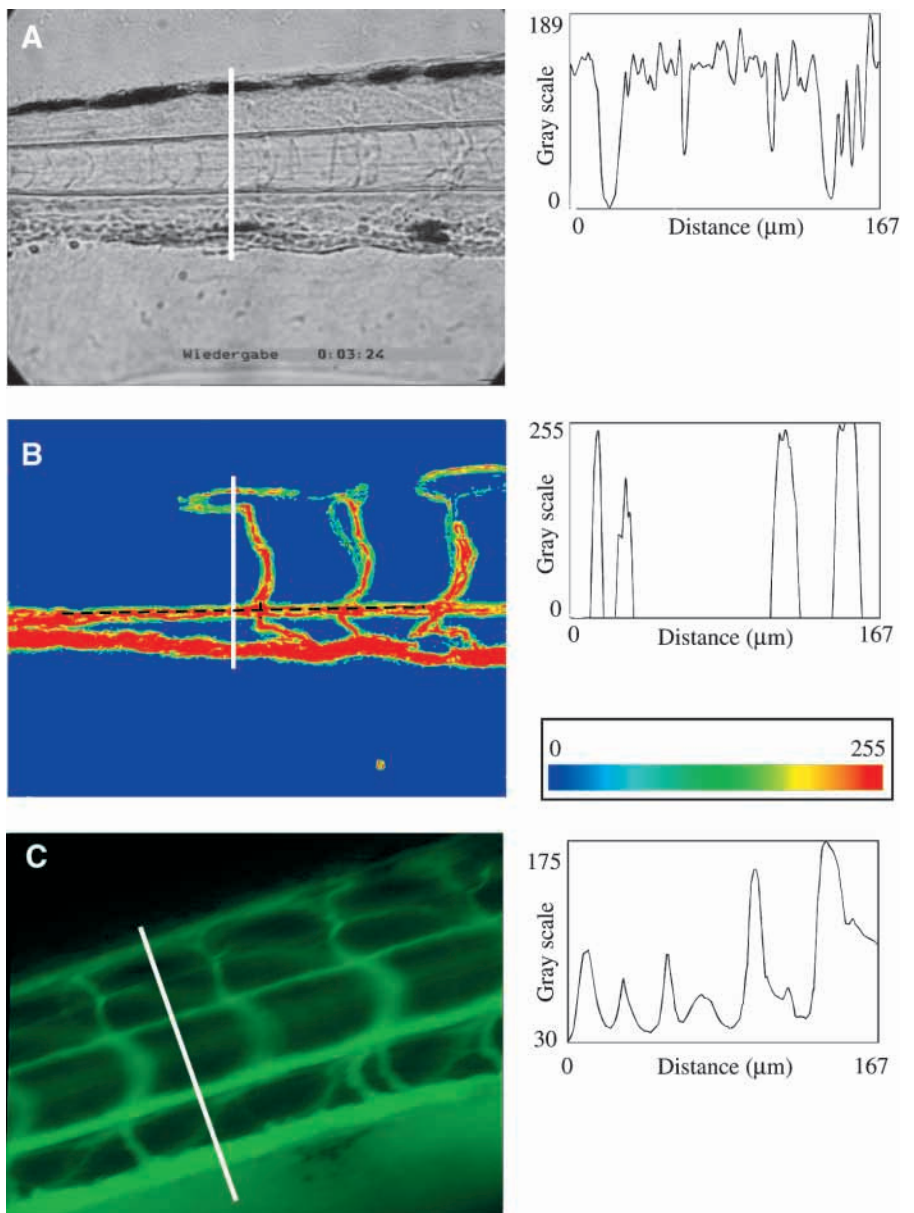


Fig. 4. (A) A typical video image showing a lateral view of the tail region of a zebrafish larva. The white bar indicates the location of a cross-sectional intensity profile of the gray-scale distribution in the tail region. The gray-scale histogram of this section (right) gives little indication of the edges of the blood vessel. (B) An uncalibrated false-colour-coded visualisation of blood vessels in the same preparation obtained by superimposing difference images from 30 consecutive video frames. The gray-scale histogram of the cross-sectional intensity profile (right) indicated by the white bar clearly marks the locations of blood vessels. The two dashed lines intersecting at the branch to the intersegmental vessel indicate the automatically detected reference point. (C) A fluorescence image of the tail region of a zebrafish embryo following an injection of FITC bound to macromolecular dextran ($M_r 5 \times 10^5$). The gray-scale histogram (right) of the cross-sectional intensity profile indicated by the white bar shows the locations of blood vessels, although the edges are somewhat blurred compared with the gray-scale histogram shown in B.

Determination of vessel diameter in video images

The diameter of blood vessels was determined on the video image by drawing an orthogonal line between the vessel walls. The measurements were made using the Optimas program package (Media Cybernetics). To compensate for possible movements that may have shifted the site of measurement between subsequent determinations, a reference point was defined in the vicinity of the measuring site. 'Landmarks' such as characteristic branching points of blood vessels were used as reference points.

The diameter of blood vessels was also determined following an intra-ventricular injection of the fluorescent probe fluorescein isothiocyanate (FITC) bound to a high-molecular-mass dextran ($M_r 5 \times 10^5$) to visualise the blood plasma. The experiments were performed with a fluorescence microscope (Zeiss Axiovert 100, Vienna, Austria). The fluorescent plasma made the measurement of vessel diameter possible by detecting the vessel walls and looking for the greatest change in contrast between the plasma and the non-fluorescent background. Once the region of interest had been defined, the complete data extraction from the images ran automatically.

Statistical analyses

Both the acquired data and the extracted data were automatically exported into an ASCII file for statistical analysis. After preprocessing the data in Microsoft Excel, statistical analyses were performed using the software package Statistica.

Results

By subtracting the odd and even fields of one video frame, shifting vectors were obtained, the length of this shifting vector for an individual object being a measure of the distance travelled by that object within the 20 ms necessary to acquire one field of a frame. As shown in Fig. 3, there was a linear correlation between the velocity of zebrafish erythrocytes determined on the basis of the length of the shifting vector and the velocity determined using the conventional frame-to-frame technique. The velocity determined by generating a shifting vector by digital motion analysis reached a maximum value at approximately $450 \mu\text{m s}^{-1}$. The erythrocytes of the eel are slightly larger than the erythrocytes of the zebrafish, and the maximum length of the shifting vector in the eel was reached at a velocity of approximately $600 \mu\text{m s}^{-1}$. Thus, in zebrafish larvae, erythrocyte velocities greater than $450 \mu\text{m s}^{-1}$ could not be measured using the digital motion analysis technique. Using the frame-to-frame technique, higher velocities could be measured as long as the density of red blood cells was low enough to identify individual cells.

In early fish larvae and in transparent animals, the blood vessels are, depending on the haematocrit and blood flow, very pale and their edges are very hard to define in video images. In still images, the edges of a vessel often almost disappear (Fig. 4A). It was not surprising, therefore, that measurements of vessel diameter showed striking variations between

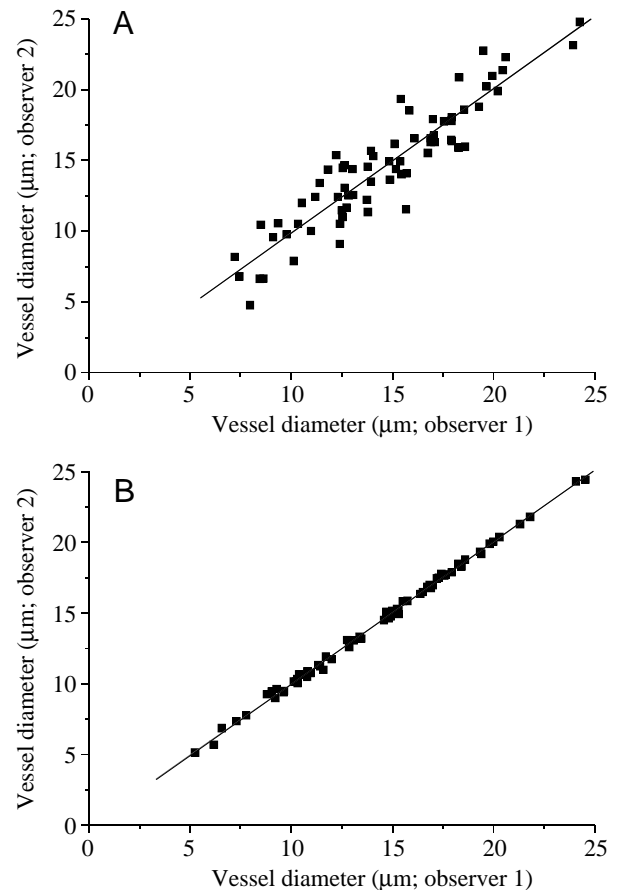


Fig. 5. (A) The diameter of blood vessels within the tail of zebrafish larvae determined by two independent observers analysing typical video images. The slope of the regression line is 1.021 ($r=0.922$). (B) The diameter of blood vessels within the tail of zebrafish larvae determined by two independent observers analysing the vascular system visualised by superimposing a sufficiently large number of shifting vectors from consecutive frames. The slope of the regression line is 1.007 ($r=0.999$).

independent observers (Fig. 5A). Even repeated diameter determinations made by the same observer gave varying results depending on the contrast, brightness and optical focus of the image. An intensity profile of an orthogonal line through a blood vessel of a typical video image revealed that, indeed, the gray-scale histogram showed no characteristic peak for object separation (Fig. 4A).

Using digital motion analysis, the vascular bed was visualised by summing images of shifting vectors from several consecutive frames. The images of the vascular bed obtained showed a clear contrast between blood vessel and background (Fig. 4B). The gray-scale histogram of such an image (Fig. 4B) clearly indicated the location of blood vessels and enabled the diameter of a vessel to be easily determined (Fig. 5B).

Blood vessel diameter in zebrafish larvae was also determined following visualisation of the vascular bed by injection of a macromolecule-bound fluorescent probe (FITC-dextran; Fig. 4C). Compared with the image obtained by digital motion

analysis, the background was much less homogeneous, and the contrast between blood vessels and background was much less pronounced. Accordingly, the gray-scale histogram was blurred at the edges of the blood vessels (Fig. 4C). Furthermore, injection of FITC-dextran turned out to be quite difficult in these tiny animals, and several hours after the injection fluorescence was always noticed in tissue cells, resulting in an increasing background signal. The fluorescence signal faded within two or three days. The cardiac activity of the larvae was often significantly reduced following the injection. Therefore, no further development of this method was attempted.

By accumulating the shifting vectors derived from moving erythrocytes, an image of the routes over which erythrocytes moved was obtained. This led to the idea that the gray-scale value of a given pixel should increase in linear proportion to the number of erythrocytes passing it, as long as the velocity of the erythrocytes or the density of erythrocytes does not exceed the time resolution of the video camera. As demonstrated in Fig. 6, there was indeed a linear correlation between the erythrocyte count achieved using the frame-to-frame technique and the erythrocyte count based on the gray-scale value obtained as a result of the digital motion analysis procedure. Thus, differences in blood distribution in whole animals could be visualised in overview images using a 4× phase-contrast objective.

Fig. 7 shows as an example the development of the vascular system in zebrafish larvae. Four days post-fertilisation, the circulatory system is operational, and erythrocytes were encountered mainly in the yolk sac, but also in the dorsal artery and vein. The head region was also well-perfused with red cells, but segmental vessels in the muscle tissue were barely detectable. At 5 days post-fertilisation, the segmental vessels were perfused with erythrocytes, and the size of the yolk sac was reduced. At 6 days post-fertilisation, the vascular system supplying the inner organs became visible, and the yolk sac was almost completely resorbed. At this stage, the erythrocytes were more evenly distributed within the vascular bed than at days 4 and 5 post-fertilisation, and this tendency became more obvious at 7 days post-fertilisation. At 7 days post-fertilisation, the swimbladder was inflated. At all stages, the ventricle could be clearly identified.

Fig. 8 shows the blood distribution in a fed and an unfed zebrafish larva at approximately 8 days post-fertilisation. In the fed larva, erythrocytes were concentrated in the gut area, indicating a good blood supply to the gut, while in the unfed animal almost no erythrocytes could be detected in the gut. In contrast, the opposite effect was observed in the intersegmental vessels. Thus, a significant redistribution of blood between the gut and the segmental muscle tissue was possible at this stage of development.

At this stage, adrenergic control of peripheral blood vessels was established in zebrafish larvae. As shown in Figs 9 and 10, application of the α -adrenergic mediator phenylephrine resulted in a significantly lower erythrocyte count in the segmental blood vessels supplying the muscle tissue. Measurement of the blood vessel revealed that the diameter of

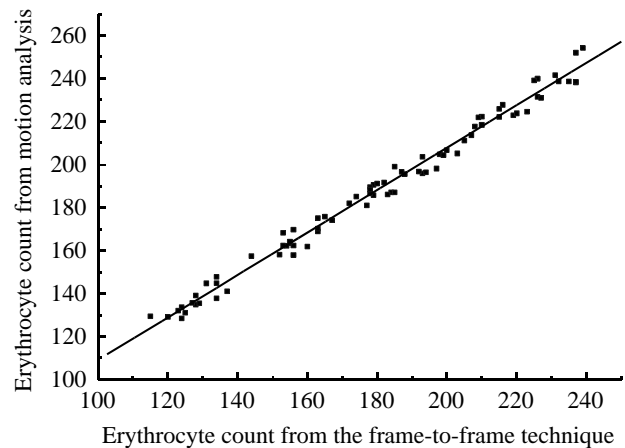


Fig. 6. The number of erythrocytes determined on the basis of the gray-scale value of the shifting vectors (motion analysis) in relation to the number of erythrocytes determined in the same preparations by counting the cells on normal video images (frame-to-frame technique). The slope of the regression line is 0.987 ($r=0.994$).

the segmental vessel in the middle region was unchanged but that, at the entrance to the segmental vessel, the diameter was significantly reduced (Fig. 10). Many erythrocytes turned into the branch but did not pass this constricted segment and returned to the dorsal artery (Fig. 9B). The first segment of the segmental artery therefore appeared to function as a 'sphincter'.

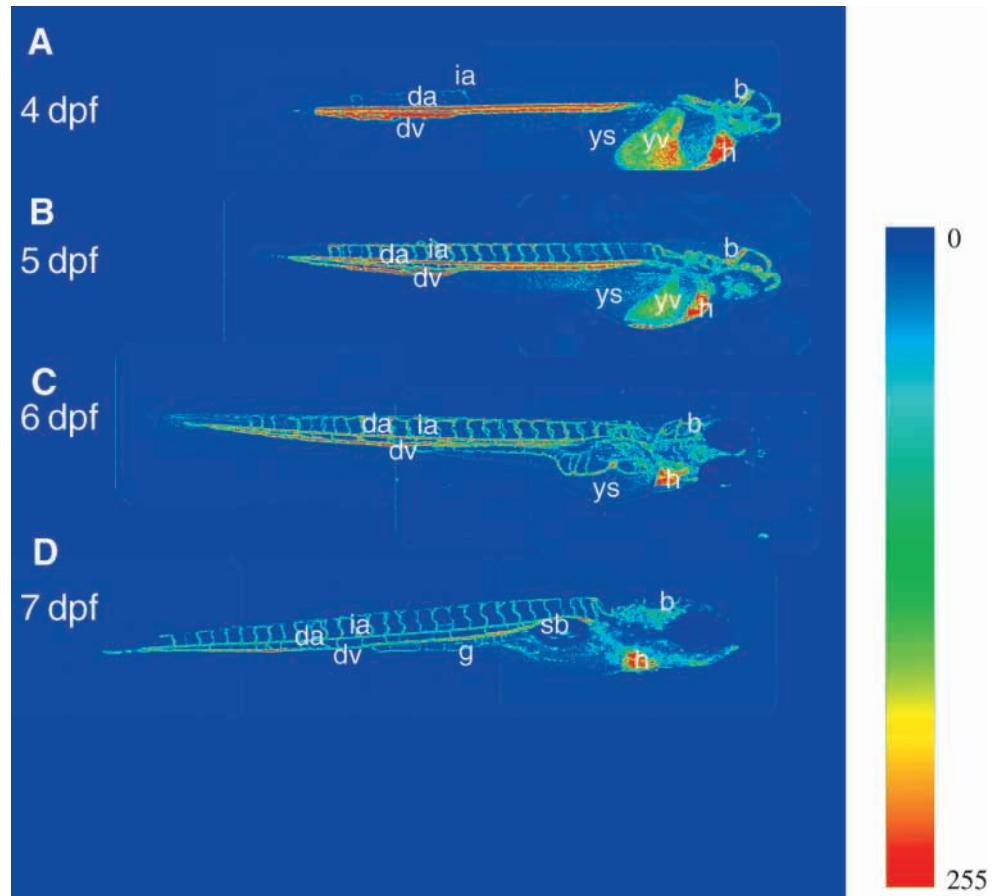
Discussion

Critique of methods

Video-microscopic analysis of cardiovascular performance requires the immobilisation of tissues, because any tissue movement shifts the region of interest and obscures the movement of red cells. In our study, we used infrared illumination and a high-viscosity agarose medium combined with light anaesthesia to prevent the movement of zebrafish larvae. Particularly in the early larval stages, the infrared illumination (band-pass filters of 780 nm and of 913 nm) proved to be very effective in settling the larvae. Compared with illumination using the full spectrum of a tungsten lamp, the larvae were significantly less active in the observation chamber and often remained quietly on the bottom, so that recordings could easily be made using the inverted microscope. The CCD cameras, which are very sensitive to these wavelengths, provided excellent images. Using infrared illumination, recordings of the cardiovascular system in zebrafish and minnow larvae (G. Schönweger, T. Schwerte and B. Pelster, in preparation) were possible until inflation of the swimbladder without any anaesthesia or physical restriction of the animals.

To visualise the vascular bed, the shifting vectors of several frames had to be superimposed, and this required the immobilisation of animals using a high-viscosity medium. A widespread method for mounting small animals for micro-

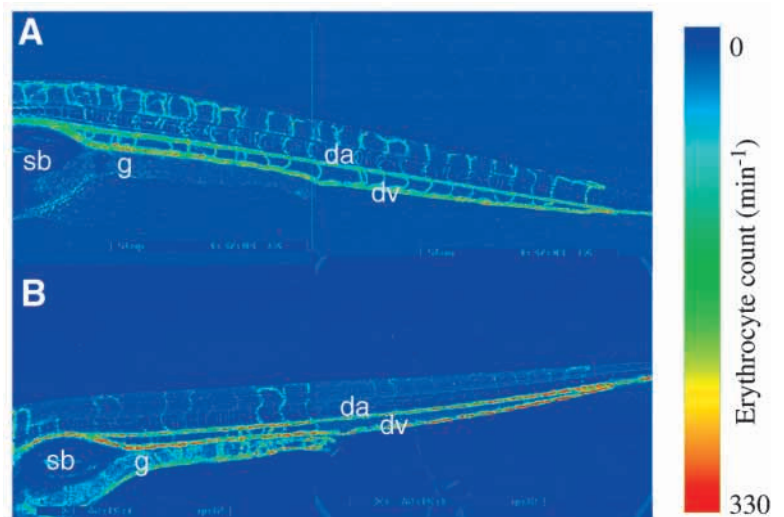
Fig. 7. Uncalibrated false-colour-coded distribution of erythrocytes in developing zebrafish larvae (4× phase-contrast objective; image width, 6.3 mm). (A) Zebrafish larva at 4 days post-fertilisation (dpf). The erythrocytes were mainly concentrated in the yolk sac and within the primary blood vessel loop in the tail forming the dorsal artery and vein. (B) Zebrafish larva at 5 days post-fertilisation. The intersegmental vessels were perfused, and blood flow over the yolk sac was reduced. (C) Zebrafish larva at 6 days post-fertilisation. Perfusion of the inner organs is now visible. The vessels are more evenly perfused compared with the earlier stages. (D) Zebrafish larva at 7 days post-fertilisation. The swimbladder is inflated, and the onset of blood flow in the swimbladder vessels is visible. da, dorsal artery; dv, dorsal vein; b, brain; g, gut; h, heart; ia, intersegmental artery; sb, swimbladder; ys, yolk sac; yv, yolk sac vein.



injections is incubation in low-melting-point agarose. The gelling temperature of the agarose (26–30°C) is within the physiological range of temperature for zebrafish. High-viscosity solutions reduce water convection and therefore increase the magnitude of unstirred layers, which significantly impairs gas exchange (Pinder and Feder, 1990; Feder and Booth, 1992). Measurements of oxygen equilibration in a 150 µm layer of 1% agarose in comparison with a layer of stirred water indeed revealed that the time necessary to

equilibrate the agarose was approximately twice as long. However, the cardiac activity of zebrafish larvae was not affected in agarose. Until 15 days after fertilisation, which is approximately the time when opercular movements start (at 25°C), heart rate, stroke volume and cardiac output were not significantly altered following agarose incubation (T. Schwerte, unpublished results). We therefore conclude that, in the early larval stages, incubation in agarose can be used to immobilise the larvae. Older zebrafish (15 days post-

Fig. 8. Calibrated false-colour-coded distribution of erythrocytes in zebrafish larvae visualised by accumulation of difference pictures generated from 30 consecutive frames in an overview image using a 4× phase-contrast objective (image width, 3.8 mm). (A) Blood distribution in an unfed zebrafish larva at approximately 8 days post-fertilisation. (B) Blood distribution in a fed larva. In the fed larva, erythrocytes are concentrated in the gut area, indicating a good blood supply to the gut. In the unfed larva, almost no erythrocytes could be detected in the gut. da, dorsal artery; dv, dorsal vein; g, gut; sb, swimbladder.



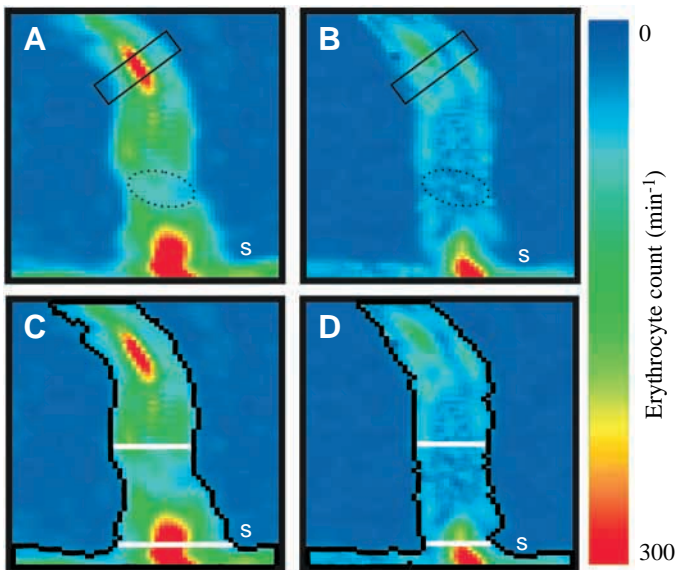


Fig. 9. Calibrated false-colour-coded distribution of erythrocytes in an intersegmental artery located in the tail region of a zebrafish larva at 8 days post-fertilisation. (A) Red cell distribution under control conditions. The entrance to the segmental vessel and a bend within the segmental vessel are 'hot spots' where, because of a transient reduction in velocity, most of the erythrocytes are encountered. (B) Red cell distribution during the application of the α -adrenergic agonist phenylephrine. The hot spot at the entrance to the segmental vessel is located closer to the dorsal artery, and the hot spot at the bend within the segmental vessel has disappeared. In the video recording, a large number of erythrocytes were observed turning briefly into the entrance of the segmental vessel, but then continuing their passage within the dorsal artery. (C,D) The diameter of the segmental vessel under control conditions (C) and following the application of phenylephrine (D) shown as an overlay of A and B. Application of phenylephrine resulted in a significant reduction in the diameter of the segmental blood vessel right at its entrance. This segment therefore functions like a 'sphincter'. The white bars indicate the sites where the diameters of the vessel shown in Fig. 10 were determined. The black rectangles indicate the region of interest where passing erythrocytes were counted; dashed ellipses indicate a position where a quantitative analysis of red cell distribution was not possible because of pigmentation of the vessel wall. s, 'sphincter' ($40\times$ phase-contrast objective; image width, $33.3\ \mu\text{m}$).

fertilisation and older), however, were significantly affected by incubation in agarose, heart rate decreasing within a few minutes.

For immobilisation, approximately $50\ \text{mg l}^{-1}$ MS222 (tricaine) was added to the water. MS222 is a known sympathetic agonist, and an overdose ($600\ \text{mg l}^{-1}$) can be used to stop the heart (Weinstein et al., 1996). The concentration used in our study was very low, and a comparison of the cardiac activity of MS222-incubated animals and control animals analysed under infrared illumination revealed no significant differences. This is in line with the results of Mirkovic and Rombough (1998), who reported that a concentration of $20\ \text{mg l}^{-1}$ suppressed spontaneous body movements in larvae of rainbow trout (*Oncorhynchus mykiss*),

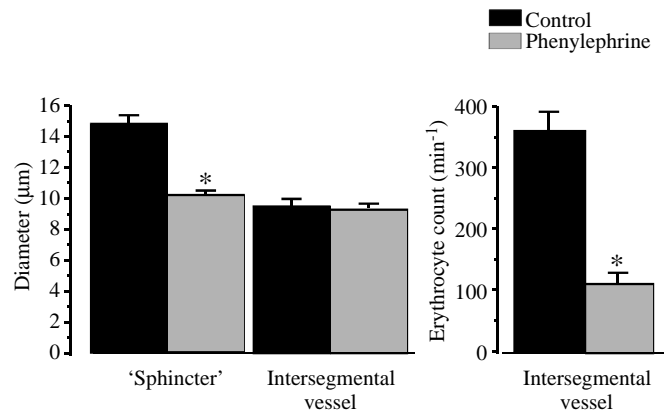


Fig. 10. Changes in vessel diameter and erythrocyte count in an intersegmental vessel located in the tail of a zebrafish larva at 8 days post-fertilisation. Measuring sites were as indicated in Fig. 9. 'Sphincter' represents the site at the entrance to the intersegmental vessel. Values are means + S.E.M., $N=12$. An asterisk indicates a significant difference between the control and the value in the presence of phenylephrine; $P<0.05$.

but had no significant effect on heart rate and on the rate of opercular movements even when applied 30 min prior to experiments. Similar results were also obtained for larvae of the clawed frog *Xenopus laevis* in which, during the early larval stages, MS222 did not affect cardiac activity (R. Fritsche, personal communication).

For measurements on very tiny vessels, the noise, even from excellent SVHS video recorders, sometimes decreases the resolution. For this reason, processing the camera signal directly provided more accurate measurements. The output from the recently available DV recorders is much closer to this live camera signal, although the video compression used sometimes produces artefacts. The programs described in this study can easily be adopted to both full- and half-frame-storing recorders.

Determination of erythrocyte velocity using digital motion analysis

Ultrasonic Doppler flowmeters are appropriate for making flow measurements on small arteries and veins. In our experience, this method is limited to vessels larger than approximately $100\ \mu\text{m}$ in diameter. Using a focused laser beam, the laser Doppler anemometer is suitable for even smaller vessels down to a diameter of approximately $10\ \mu\text{m}$ (Stücker et al., 1996). Using Doppler flowmetry, the signal-to-noise ratio decreases severely at low velocities and, especially with ultrasound, low velocities are very difficult to measure. The digital motion analysis technique can easily detect very slow movements but is limited in the upper range of velocities. The shifting vector generated by subtraction of the odd and even fields of a video frame cannot be longer than the moving object; therefore, the maximum velocity that can reliably be measured is the diameter of an erythrocyte per 20 ms. For zebrafish larvae, the maximum velocity was approximately $450\ \mu\text{m s}^{-1}$, while for eel erythrocytes a velocity of $600\ \mu\text{m s}^{-1}$

was measurable. The low range of velocities is simply limited by the pixel size. Like Doppler flowmetry, digital motion analysis provides information about instantaneous velocities, but it also permits the velocity of a single erythrocyte to be determined and, by integrating the velocity signal over several erythrocytes and/or over a user-defined time window, for example, allows cardiac-cycle-dependent velocity fluctuations to be eliminated.

Thus, digital motion analysis lends itself particularly to the analysis of red cell velocity in small transparent animals. Compared with the conventional frame-to-frame technique, it also has the advantage that it is much less dependent on the illumination and contrast of the preparation. Digital motion analysis is not observer-dependent, and this significantly increases the accuracy of the measurements. Furthermore, the analysis is much easier and less time-consuming and the velocity morphometric data on the blood vessels can be acquired almost simultaneously.

Visualisation of blood vessels

Small blood vessels in fish and amphibian larvae often have a very low contrast, and the diameter estimations even of experienced observers show large variations. This may in part be due to minor misplacements of the optical focus or to changes in the contrast and brightness of the image. The proportional error increases with a decrease in vessel diameter. Visualisation of a blood vessel by superimposing shifting vectors calculated from several frames generates a very good image of the vessel, with sharp edges, which is insensitive to minor changes in the optical focus. The disadvantage of this method is that it visualises only those vessels in which erythrocytes are encountered and it may underestimate the diameter of a vessel as a result of axial red cell accumulation and plasma sleeving (Schmid-Schönbein, 1988). This effect occurs in the presence of a tiny layer of erythrocyte-free plasma at the surface of the endothelium. On the basis of model calculations about red cell movements in a capillary system, this plasma layer is estimated to have a thickness of approximately 1 μm or less (Schmid-Schönbein, 1988). To evaluate the accuracy of our method, we compared the blood vessel thickness determined from the accumulated difference images with the diameter measured from a complete video image of the same site. The results differed by approximately 2–3%. We conclude, therefore, that using the movement of the red cells to create a picture of the vascular bed is an extremely useful method of analysing the vascular system in larval fish.

Compared with the normal video image, the use of high-molecular-mass fluorescent probes to visualise blood plasma creates better images of the vascular system, but the gray-scale histogram of such an image shows the edges of a blood vessel less clearly than the gray-scale histogram of an image generated using digital motion analysis. Compared with the use of fluorescent probes, our method opens up the possibility of visualising the development of the vascular bed and the capillarization of tissues in long-term experiments. While fluorescent probes fade after a few days and apparently can

even be taken up by cells, the visualisation of blood vessels by summing shifting vectors of erythrocytes is not invasive and can be performed repeatedly in the same animal over a period of days or even weeks, depending on how much the pigmentation of the skin increases. In contrast to fluorescence microscopy, the use of laser scanning microscopes provides a much better spatial resolution that enables a three-dimensional reconstruction of whole vessels. But, for this imaging technique, fluorescent probes have to be injected, which is very invasive (see above). Furthermore, because of the higher light intensities required, the fading effect is much higher than for wide-field fluorescence microscopy, and the use of anti-fading agents in living animals is problematic.

Especially in long-term experiments, the relocalization of the region of interest is critical. For morphometric analysis of an image, orientation of the vascular system according to landmarks (bends in a vessel or vessel bifurcations) is an accepted procedure (MacFarlane et al., 1983; Vesely et al., 1990; Sundin, 1995; Sundin and Nilsson, 1997; Hanger et al., 1995; Hudetz, 1997; Nakazawa and Kajio, 1997). Often it is not the landmark itself where the measurement takes place, and minor errors in the exact relocalization may well contribute to the observed scatter in morphometric measurements (see Fig. 5A). Using our method, this problem is easily alleviated by defining a reference point which is automatically relocalized by the computer prior to each measurement.

Visualisation of erythrocyte distribution

Measurement of erythrocyte velocity using the frame-to-frame technique is possible in smaller blood vessels in which single blood cells can be observed, and this technique may therefore also be used to count the number of red cells present in a particular region of a blood vessel. Especially at high flow rates, counting erythrocytes is very difficult, and counting them using the frame-to-frame technique is very time-consuming. Motion-based image analysis permits red blood cells to be counted in real time because the gray-scale value of any pixel in the superimposed difference image is correlated to the number of erythrocytes encountered during the measurement. Thus, the distribution of erythrocytes within a tissue or within a larva can easily be visualised. Our experiments nicely describe the development of the peripheral vascular system in zebrafish larvae. At the time of first feeding (at 7 or 8 days post-fertilisation), food intake already resulted in a clear redistribution of blood between muscle tissue and the gut. One way of achieving a redistribution of blood is the selective distribution and activation of α - and β -adrenergic receptors within the peripheral circulation. The reduction in the red cell count within segmental blood vessels following the application of phenylephrine clearly demonstrates that this mechanism is already established in zebrafish larvae at 8 days post-fertilisation. In additional experiments, we were also able to show that the peripheral vascular system of zebrafish larvae at this stage responds to nitric oxide (R. Fritsche, T. Schwerte and B. Pelster, in preparation).

In summary, the present study demonstrates that the

visualisation of erythrocyte movements by subtracting the two fields of a video frame provides a very effective tool not only for measuring erythrocyte velocity and blood flow in transparent embryos and larvae of lower vertebrates but also for visualising the capillary bed and the distribution of red cells within the vascular system. As a non-invasive technique, it can also be used for long-term observations to visualise angiogenesis and vasculogenesis in growing embryos and larvae.

The study was financially supported by the Fonds zur Förderung der wissenschaftlichen Forschung (FWF, P12571-BIO).

References

- Burggren, W. W. and Fritsche, R.** (1995). Cardiovascular measurements in animals in the milligram range. *Braz. J. Med. Biol. Res.* **28**, 1291–1305.
- Colmorgen, M. and Paul, R. J.** (1995). Imaging of physiological functions in transparent animals (*Agonus cataphractus*, *Daphnia magna*, *Pholcus phalangioides*) by video microscopy and digital image processing. *Comp. Biochem. Physiol.* **111A**, 583–595.
- Faber, J. J., Green, T. J. and Thornburg, K. L.** (1974). Embryonic stroke volume and cardiac output in the chick. *Dev. Biol.* **41**, 14–21.
- Fagrell, B., Fronek, A. and Intaglietta, M.** (1977). A microscope–television system for studying flow velocity in human skin capillaries. *Am. J. Physiol.* **233**, H318–H321.
- Farrell, A. P., Sobin, S. S., Randall, D. J. and Crosby, S.** (1980). Intralamellar blood flow patterns in fish gills. *Am. J. Physiol.* **239**, R428–R436.
- Feder, M. E. and Booth, D. T.** (1992). Hypoxic boundary layers surrounding skin-breathing aquatic amphibians: occurrence, consequences and organismal responses. *J. Exp. Biol.* **166**, 237–251.
- Fritsche, R. and Burggren, W. W.** (1996). Development of cardiovascular responses to hypoxia in larvae of the frog *Xenopus laevis*. *Am. J. Physiol.* **271**, R912–R917.
- Hanger, C. C., Hillier, S. C., Presson, R. G. J., Glenney, R. W. and Wagner, W. W. J.** (1995). Measuring pulmonary microvessel diameters using video image analysis. *J. Appl. Physiol.* **79**, 526–532.
- Hou, P. C. L. and Burggren, W. W.** (1995). Cardiac output and peripheral resistance during larval development in the anuran amphibian *Xenopus laevis*. *Am. J. Physiol.* **269**, R1126–R1132.
- Hudetz, A. G.** (1997). Blood flow in the cerebral capillary network: A review emphasizing observations with intravital microscopy. *Microcirculation* **4**, 233–252.
- Hughes, G. M., Horimoto, M., Kikuchi, Y., Kakiuchi, Y. and Koyama, T.** (1981). Blood-flow velocity in microvessels of the gill filaments of the goldfish (*Carassius auratus* L.). *J. Exp. Biol.* **90**, 327–331.
- Keller, B. B., MacLennan, M. J., Tinney, J. P. and Yoshigi, M.** (1996). *In vivo* assessment of embryonic cardiovascular dimensions and function in day-10.5 to -14.5 mouse embryos. *Circ. Res.* **79**, 247–255.
- Koyama, T., Mishina, H. and Asakura, T.** (1975). A study of microcirculation in web of frog (*Xenopus laevis* Daudin) by using laser Doppler microscope. *Experientia* **31**, 1420–1422.
- MacFarlane, T. W., Petrowski, S., Rigutto, L. and Roach, M. R.** (1983). Computer-based video analysis of cerebral arterial geometry using the natural fluorescence of the arterial wall and contrast enhancement techniques. *Blood Vessels* **20**, 161–171.
- Mirkovic, T. and Rombough, P.** (1998). The effect of body mass and temperature on the heart rate, stroke volume and cardiac output of larvae of the rainbow trout, *Oncorhynchus mykiss*. *Physiol. Zool.* **71**, 191–197.
- Nakazawa, M. and Kajio, F.** (1997). Hormonal systems regulating the developing cardiovascular system. In *Development of Cardiovascular Systems* (ed. W. W. Burggren and B. B. Keller), pp. 88–98. Cambridge: Cambridge University Press.
- Nilsson, G.E., Löfman, C.O. and Block, M.** (1995). Extensive erythrocyte deformation in fish gills observed by *in vivo* microscopy: apparent adaptations for enhancing oxygen uptake. *J. Exp. Biol.* **198**, 1151–1156.
- Orlando, K. and Pinder, A. W.** (1995). Larval cardiorespiratory ontogeny and allometry in *Xenopus laevis*. *Physiol. Zool.* **68**, 63–75.
- Pelster, B.** (1994). Adrenergic control of swimbladder perfusion in the European eel *Anguilla anguilla*. *J. Exp. Biol.* **189**, 237–250.
- Pelster, B. and Bemis, W. E.** (1992). Structure and function of the external gill filaments of embryonic skates (*Raja erinacea*). *Respir. Physiol.* **89**, 1–13.
- Pinder, A. W. and Feder, M. E.** (1990). Effect of boundary layers on cutaneous gas exchange. *J. Exp. Biol.* **143**, 67–80.
- Schmid-Schönbein, H.** (1988). Fluid dynamics and hemorrheology *in vivo*: The interactions of hemodynamic parameters and hemorrheological ‘properties’ in determining the flow behavior of blood in microvascular networks. In *Clinical Blood Rheology*, vol. 1 (ed. G. D. O. Lowe), pp. 129–219. Boca Raton, FL: CRC Press.
- Schwerte, T., Axelsson, M., Nilsson, S. and Pelster, B.** (1997). Effects of vagal stimulation on swimbladder blood flow in the European eel *Anguilla anguilla*. *J. Exp. Biol.* **200**, 3133–3139.
- Stensløkken, K.-O., Sundin, L. and Nilsson, G. E.** (1999). Cardiovascular and gill microcirculatory effects of endothelin-1 in Atlantic cod: evidence for pillar cell contraction. *J. Exp. Biol.* **200**, 1151–1157.
- Stücker, M., Baier, V., Reuther, T., Hoffmann, K., Kellam, K. and Altmeyer, P.** (1996). Capillary blood cell velocity in human skin capillaries located perpendicularly to the skin surface: measured by a new laser Doppler anemometer. *Microvasc. Res.* **52**, 188–192.
- Sundin, L.** (1995). Serotonergic vasomotor control in fish gills. *Braz. J. Med. Biol. Res.* **28**, 1217–1221.
- Sundin, L. and Nilsson, G. E.** (1997). Neurochemical mechanisms behind gill microcirculatory responses to hypoxia in trout: *in vivo* microscopy study. *Am. J. Physiol.* **272**, R576–R585.
- Vesely, I., Menkis, A. and Campbell, G.** (1990). A computerized system for video analysis of the aortic valve. *IEEE Trans. Biomed. Eng.* **37**, 925–929.
- Weinstein, B. M., Schier, A. F., Abdelilah, S., Malicki, J., Solnica-Krezel, L., Stemple, D. L., Stainier, D. Y. R., Zwartkruis, F., Driever, W. and Fishman, M. C.** (1996). Hematopoietic mutations in the zebrafish. *Development* **123**, 303–309.